Fuel 229 (2018) 151–166

Contents lists available at ScienceDirect

Fuel

journal homepage: www.elsevier.com/locate/fuel

Full Length Article

Characterization of pyrolysis products from fast pyrolysis of live and dead vegetation native to the Southern United States

Mohammad-Saeed Safdari[a], Mahmood Rahmati[a], Elham Amini[a], Joel E. Howarth[a], Jansen P. Berryhill[a], Mark Dietenberger[b], David R. Weise[c], Thomas H. Fletcher[a,*]

[a] Chemical Engineering Department, Brigham Young University, Provo, UT 84602, USA
[b] USDA Forest Service, Forest Products Laboratory, Madison, WI 53726, USA
[c] USDA Forest Service, PSW Research Station, Fire and Fuels Program, Riverside, CA 92507, USA

GRAPHICAL ABSTRACT

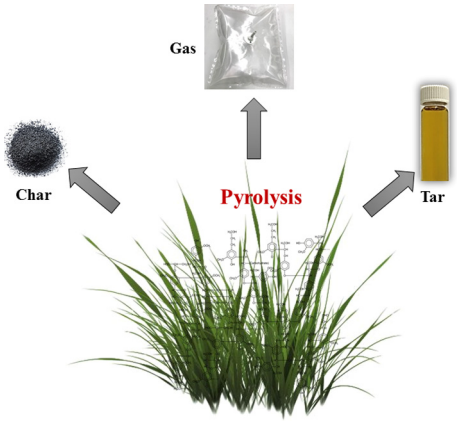

ARTICLE INFO

Keywords:
Pyrolysis
Live plant
Biomass
Char
Tar
Light gas

ABSTRACT

Prescribed burning (controlled burning) is used to decrease accumulation of combustible materials and reduce impact of uncontrolled wildland fires. Prescribed fires are often used to burn undergrowth in Southern forests of the United States. In order to improve prescribed fire application, accomplish desired fire effects, and limit potential runaway fires, an improved understanding of the fundamental processes related to combustion of heterogeneous fuel beds of live and dead fuels is needed. The initial processes of combustion involve pyrolysis and ignition. During this research, fast pyrolysis of 14 live and dead (biomass) plant species which are native to the Southern United States have been studied using a flat-flame burner (FFB) apparatus. The FFB apparatus enables experiments at a high heating rate (~100 °C s^{-1}, or ~100 kW m^{-2}) and moderate temperature (~765 °C) to imitate pyrolysis during typical fire spread conditions. Pyrolysis products have been analyzed in detail using a gas chromatograph equipped with a mass spectrometer (GC–MS) for analysis of tars, and a gas chromatograph equipped with a thermal conductivity detector (GC-TCD) for analysis of permanent (light or non-condensable) gases. Differences between yields of light gas species were small between plant species. Composition of tars included aromatic compounds with 1–5 rings with very few attachments. The pyrolysis products observed at this temperature and heating rate appear to have experienced secondary pyrolysis. The tar composition showed some large changes with plant species. Comparison of products from pyrolysis of live

* Corresponding author at: 350 CB, BYU, Provo, UT 84602, USA.
E-mail address: tom_fletcher@byu.edu (T.H. Fletcher).

https://doi.org/10.1016/j.fuel.2018.04.166
Received 23 February 2018; Received in revised form 20 April 2018; Accepted 28 April 2018

vegetation and dead vegetation of the same plant species showed differences in tar, gas, and char yields, but no major changes in the types of chemical compounds observed.

1. Introduction

Wildland fire is an important component of many ecosystems. Wildland fires often occur in highly dense live fuel forests, burn live and dead vegetation, and have significant ecological and economic impacts [1]. In 2000, an estimated 3.5 million km^2 were burned by wildland fire world-wide [2]. Prescribed burning (controlled burning) is one way to remove smaller plants in order to decrease accumulation of combustible materials and avoid occurrence of uncontrolled wildland fires [3]. The land managers use prescribed fire to manage a variety of ecosystems in the United States to reduce accumulation of hazardous fuels, manage wildlife habitat, and protect ecological forests and infrastructures [4]. In 2014, in the United States, an estimated 47,372 km^2 were treated with prescribed fire; in the southern U.S., 25,051 km^2 of forest land was treated [5]. Prescribed fires (as shown in Fig. 1) are often used to burn undergrowth in Southern forests of the United States.

During wildland fires, solid fuel samples undergo irreversible thermal degradation when exposed to high temperatures. The thermal degradation process consists of two sequential steps: pyrolysis and combustion [6]. In order to improve prescribed fire application, accomplish desired fire effects, and limit potential runaway fires, an improved understanding of the fundamental processes related to pyrolysis and ignition in heterogeneous fuel beds of live and dead fuels is needed.

The focus of this research is on pyrolysis, which is the first thermochemical reaction that occurs following the evaporation of moisture in the burning of some fuels like coal, wood, paper, polymers, plants, etc. As volatiles leave the surface, the mass transfer pushes the surrounding gas (presumably air) out of the way, creating a fuel-rich zone near the surface or in the interior of a flame. The results from this research can help to determine the heat release and investigate reactions that occur during the fast pyrolysis of live and dead vegetation. Finding mechanisms of formation of pyrolysis products helps to prepare more accurate combustion and fire spread models to predict the best conditions to properly perform prescribed burning, predict fire propagation, and limit fire runaway.

Pyrolysis is the thermal decomposition process of organic material without requiring oxygen. Flames occur when pyrolysis products and oxygen mix in the presence of an ignition source at high temperatures within the flammability limits. For example, by increasing temperature, lignocellulosic materials start to pyrolyze, releasing gaseous products which react with oxygen and may result in a flame. Pyrolysis can be classified into three groups: (1) conventional or slow pyrolysis which is performed with a slow heating rate (0.1–1 $^{\circ}C\,s^{-1}$), low temperature (300–400 °C), and long gas and solid residence time (more than 30 min); (2) fast pyrolysis which is operated with a fast heating rate (1–100 $^{\circ}C\,s^{-1}$), high temperature (500–900 °C), and short gas and solid residence time (10–20 s); and (3) flash pyrolysis which is operated under a very high heating rate (more than 1000 $^{\circ}C\,s^{-1}$) and very short residence time (1 s) [7,8].

Pyrolysis of solid fuels includes two main steps: primary and secondary pyrolysis. In primary pyrolysis, the solid fuel degrades into volatile gases and char. The primary pyrolysis products of solid fuels are non-condensable (light) gases (e.g., CO, CO_2, H_2O, and H_2), light hydrocarbons (e.g., CH_4, C_2H_4), condensable gases (tars), solid residue (char), and mineral ash. If the products of primary pyrolysis undergo further reactions at higher temperatures and longer residence times, it is known as secondary pyrolysis. Secondary pyrolysis includes processes such as cracking, polymerization, condensation, and carbon deposition, which can occur either homogeneously (when reactants are in the gas phase), or heterogeneously (when the reactions occur at the surface of a solid fuel or char particle). Secondary pyrolysis is not as widely studied as primary pyrolysis, but some secondary reactions, such as tar cracking, can have significant effects on the distribution of products [9]. During secondary pyrolysis, the tars heat up in the flame and either decompose to lighter gases or polymerize to form soot. The orange color of flames is due to the radiation from the tiny soot particles in the fuel-rich part of the flame [10]. Yields of tar and total volatiles, as well as distribution of volatile species, depend on heating rate, temperature, fuel type, etc. [11].

Pyrolysis of biomass (dead and dried vegetation) and wood have been explored in detail [10,12–14]. However, there are insufficient research studies in the field of pyrolysis of live plants. Live and dead plants burn differently [15]. A plant is considered dead when the dry-basis moisture content is less than 30 wt%, but may be as low as 4%. Dead fuels may have a moisture content higher than 35 wt% only when water from the surface of the leaf is absorbed into the cell cavities [16]. Dry-basis moisture content of live fuels may exceed 250 wt% which causes significant amounts of water to remain in the fuel during ignition. Wet dead fuels absorb water in their cell walls, and by heating the fuels, this vapor diffuses out. However, in live fuels, some of the unevaporated water expands rapidly causing the cell walls to burst [1,17]. Moisture content in live fuels converts to water vapor, dilutes the gaseous pyrolyzates and has noticeable effects on flame behavior by slowing down the burning rate [3]. In addition, it has been suggested that components such as non-structural carbohydrates, fats, and other components may impact combustion behavior of live fuels, but are not usually found in dead fuels [18–20].

Biomass pyrolysis consists of 4 main steps; moisture evolution, hemicellulose, cellulose, and then lignin decomposition [21]. Hemicellulose, cellulose, and lignin are biopolymers that form plant cell walls. The temperature range of pyrolysis for hemicellulose, cellulose, and lignin is 180–240, 230–310, and 300–400 °C, respectively, depending on heating rate [8]. At temperatures lower than 180 °C, biomass is primarily stable and pyrolysis does not occur [22]. In addition to lignocellulosic materials, live plants contain significant fractions of proteins, starches, sugars, and lipids [23].

During this research, fast pyrolysis of 14 live and dead plant species which are native to the Southern United States have been studied using a flat-flame burner (FFB) apparatus. The FFB apparatus enables experiments at high heating rates and high temperatures to imitate prescribed fire conditions under a convective heating mode only. Distribution of pyrolysis products was studied at high heating rates using a gas chromatograph equipped with a mass spectrometer

Fig. 1. Prescribed burning of the southern forests of the U.S.

Table 1
List of plants used in pyrolysis experiments.

Common name	Scientific name	Picture
Darrow's blueberry	*Vaccinium darrowii*	
Dwarf palmetto	*Sabal minor*	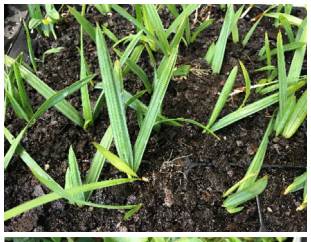
Fetterbush	*Lyonia lucida*	
Inkberry	*Ilex glabra*	
Live oak	*Quercus virginiana*	
Little bluestem grass	*Schizachyrium scoparium*	
Longleaf pine	*Pinus palustris*	

Table 1 (*continued*)

Common name	Scientific name	Picture
Pine straw (Longleaf pine litter)	*Pinus palustris*	
Saw palmetto	*Serenoa repens*	
Sparkleberry	*Vaccinium arboreum*	
Swamp bay	*Persea palustris*	
Water oak	*Quercus nigra*	
Wax myrtle	*Morella cerifera*	
Wiregrass	*Aristida stricta*	

(*continued on next page*)

Table 1 (*continued*)

Common name	Scientific name	Picture
Yaupon	*Ilex vomitoria*	

(GC–MS) for analysis of tars, and a gas chromatograph equipped with a thermal conductivity detector (GC-TCD) for analysis of light gases.

2. Material and methods

For each plant species, pre-burn measurements such as proximate and ultimate analysis as well as physical measurements were performed. The pyrolysis of both live and dead plants was studied and factors such as temperature, heating rate, and change of mass over time were measured. In addition, the products of pyrolysis, including tars and light gases, were collected and analyzed using GC–MS and GC-TCD, respectively.

2.1. Fuels tested

Live potted plants of 14 different species, as listed in Table 1, were grown in a nursery and then express-mailed to the combustion laboratory at Brigham Young University (BYU) for pyrolysis experiments. The plants were kept in a location with sufficient sunlight and water to keep them alive. Two of the plant species were grasses (little bluestem and wiregrass), one was a needle-like species (longleaf pine), and the other plants were broadleaf species. In addition, longleaf pine litter (i.e., pine straw) was studied and compared with the live and 1-week old dead longleaf pine foliage data.

In addition, before performing experiments, initial mass of the samples, proximate analysis (including moisture, ash, fixed carbon, and volatile content), ultimate analysis (or elemental analysis), and physical measurements (including width, length and thickness of the leaves and stem) were performed.

2.2. Proximate and ultimate analysis

The moisture content of the plant samples was measured using a Computrac MAX 1000 moisture analyzer. The proximate and ultimate analysis were measured by the University of Wisconsin Forage Laboratory according to ASTM D7582 and ASTM D5291 procedures, and the results are shown in Table 2. In addition, high and low heat values were measured using the ASTM E711 procedure.

The proximate analysis revealed that the foliage samples were generally similar. For the live plants, the moisture content ranged from 114 to 239 wt% (dry basis). In contrast, the moisture content of the longleaf pine litter was only 15 wt%. Ash content (silica) ranged from a low of 1.65 wt% for saw palmetto to a high of 4.33 wt% for yaupon. While the two grasses (little bluestem grass and wiregrass) had similar ash content, other closely related species differed in ash content (e.g., inkberry and yaupon, saw palmetto and dwarf palmetto). Volatile material ranged from 75.2 to 87.2 wt%. The fixed carbon (FC) ranged from a low of 9.9 wt% for dwarf palmetto to a high of 23.2 wt% for saw palmetto. Proximate analysis of the palmettos were similar to the results for date palm (*Phoenix dactylifera*) [24]. Ultimate analysis of the plants yielded no surprises in that the elemental composition of the foliage fell within the accepted ranges. The C and N content of the fetterbush and inkberry agreed well with published values [25]. The longleaf pine litter contained twice as much H as the fresh foliage and 5 percent less O.

2.3. Physical measurement

The blade thickness of the leaves (not including central vein) was measured using a caliper. The width of the leaves was measured at their widest point. In addition, the length of the leaves was measured, which included the leaf blade and the leaf petiole. Stem thickness was measured at various points along the stem except for longleaf pine which was provided as a “plug seedling” and did not have a pronounced stem [26]. The results of the physical measurements are shown in Table 3. The results are the averages of at least three measurements including ± 95% confidence intervals.

Table 2
Proximate and ultimate analysis of plant species.

Common name	MC[1]	Proximate analysis[2]			Ultimate analysis[3]						
		Ash	VM	FC	C	H	N	S	O	LHV	HHV
Darrow’s blueberry	104	2.85	n.a.	n.a.	n.a.	n.a.	n.a.	n.a.	n.a.	n.a.	n.a.
Dwarf palmetto	164	3.26	89.8	10.2	47.36	5.93	2.14	0.66	43.91	19.04	20.61
Fetterbush	91	2.24	77.7	22.3	54.36	5.81	0.80	0.12	38.91	19.00	20.57
Inkberry	85	1.88	80.2	19.8	54.63	6.42	0.87	0.11	37.97	20.94	22.52
Live oak	103	2.71	80.9	19.1	49.57	6.01	2.30	0.15	41.97	18.21	19.81
Little bluestem	217	4.12	84.9	15.1	51.22	5.66	2.22	0.15	40.75	17.63	19.09
Longleaf pine foliage	207	2.02	79.7	20.3	51.37	3.00	1.21	0.11	44.31	19.26	20.11
Longleaf pine litter	111	1.77	78.3	21.7	52.31	6.09	2.31	0.06	39.23	19.59	21.10
Saw palmetto	112	3.19	76.4	23.6	49.49	5.48	0.90	0.17	43.96	19.09	20.56
Sparkleberry	103	3.10	79.0	21.0	52.49	7.71	0.74	0.16	38.90	18.96	20.90
Swamp bay	116	1.84	79.6	20.4	52.48	6.11	1.36	0.17	39.88	20.50	22.10
Water oak	170	4.18	80.6	19.4	50.06	5.57	1.47	0.10	42.80	18.23	19.96
Wax myrtle	118	2.41	77.4	22.6	50.65	5.44	2.31	0.14	41.46	19.98	21.36
Wiregrass	135	4.34	81.7	18.3	47.42	6.34	3.31	0.25	42.68	17.74	19.34
Yaupon	104	4.89	86.2	13.8	51.34	6.28	1.46	0.18	40.74	19.79	21.43

n.a. means not available.

[1] MC (moisture content wt% dry basis) of samples used in experiment at BYU.

[2] VM (volatile material), FC (fixed carbon). Values are wt% dry-ash free. ASTM D7582.

[3] C, H, N, S, O – values are % dry mass; LHV – low heating value, HHV – high heating value (kJ g^{-1}, dry-ash free basis). ASTM D5291, D4239, E711.

Table 3
Physical measurements.

Common name	Thickness of leaves (mm)	Length of leaves (mm)	Width of leaves (mm)	Thickness of stem (mm)	Width/Length ratio
Darrow's blueberry	0.23* ± 0.06†	22 ± 5	7 ± 4	0.7 ± 0.4	0.32
Dwarf palmetto	0.21 ± 0.04	120 ± 25	9 ± 3	–	0.08
Fetterbush	0.20 ± 0.08	27 ± 6	15 ± 4	1.2 ± 0.4	0.56
Inkberry	0.32 ± 0.06	29 ± 5	15 ± 3	2 ± 0.8	0.52
Live oak	0.33 ± 0.05	61 ± 9	29 ± 6	3 ± 1.2	0.48
Little bluestem grass	0.11 ± 0.03	175 ± 67	2.3 ± 0.6	–	0.01
Longleaf pine foliage	0.42 ± 0.04	106 ± 4	–	–	–
Longleaf pine litter	0.46 ± 0.03	104 ± 4	–	–	–
Saw palmetto	0.22 ± 0.06	95 ± 22	14 ± 4	–	0.15
Sparkleberry	0.24 ± 0.05	20 ± 4	8 ± 2	0.6 ± 0.2	0.40
Swamp bay	0.30 ± 0.06	104 ± 8	27 ± 4	3.4 ± 0.5	0.26
Water oak	0.18 ± 0.03	63 ± 17	16 ± 7	2.2 ± 0.8	0.25
Wax myrtle	0.19 ± 0.04	33 ± 4	12 ± 2	0.7 ± 0.2	0.36
Wiregrass	0.31 ± 0.04	154 ± 49	–	–	–
Yaupon	0.31 ± 0.09	11 ± 3	6 ± 2	1.4 ± 0.2	0.55

* Average.
† 95% confidence interval.

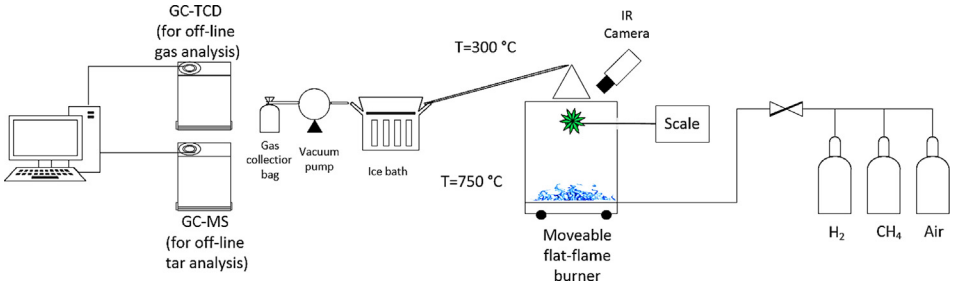

Fig. 2. Flat-flame burner (FFB) apparatus.

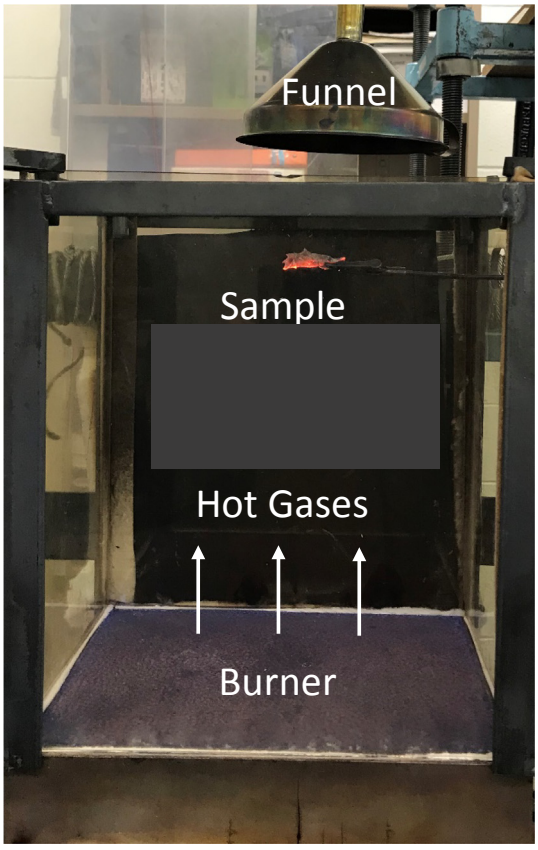

Fig. 3. Photo of the flat-flame burner apparatus with flame and pyrolyzing sample.

2.4. Experimental setup and procedure

In order to simulate pyrolysis of live and dead vegetation in wildland fires, pyrolysis experiments were performed using the flat-flame burner (FFB) apparatus to investigate the distribution of pyrolysis products at high heating rate (~100 °C s^{-1}) and moderate gas temperature (~765 °C). Experiments were performed both on live and dead samples. For live plants, the experiments were performed immediately after cutting the plants from their roots while they had very high moisture contents, which sometimes exceeded 100 wt% (dry basis). For dead plants (biomass), the samples were cut and then allowed to dry out at room temperature for about a week until their moisture content decreased to ~5 wt% before running experiments.

The FFB apparatus (Figs. 2 and 3) provides high heating rate to represent fast pyrolysis. Previous researchers used a similar setup at Brigham Young University to study: (1) the influence of seasonal change and heating mode on wildland fire behavior [27]; (2) live fuel combustion properties [28]; (3) semi-empirical modeling for fire spread in shrub fuels [29]; (4) difference in burning behavior of live and dead leaves [30].

In order to provide pyrolysis conditions and an oxygen-free environment (no combustion), the FFB was operated in a fuel-rich mode (equivalence ratio: $\Phi = 1.13$). The fuel was a mixture of methane (26.5 L min^{-1}) and hydrogen (16.6 L min^{-1}). Air (258.8 L min^{-1}) was used as an oxidizer. The samples were exposed to convective heat transfer from the post-flame products of the burner (CO_2, H_2O, and CO). No flaming or smoldering of the plant samples were observed during the experiments since the FFB was operated in fuel-rich mode. The average gas temperature within the FFB at the height where the sample was loaded was measured to be 765 °C by an OMEGA K-type thermocouple (wire diameter of 0.38 mm, response time of 0.8 s, and maximum working temperature of 871 °C), corrected for radiation losses.

A heat flux meter was also used to measure radiative, convective and

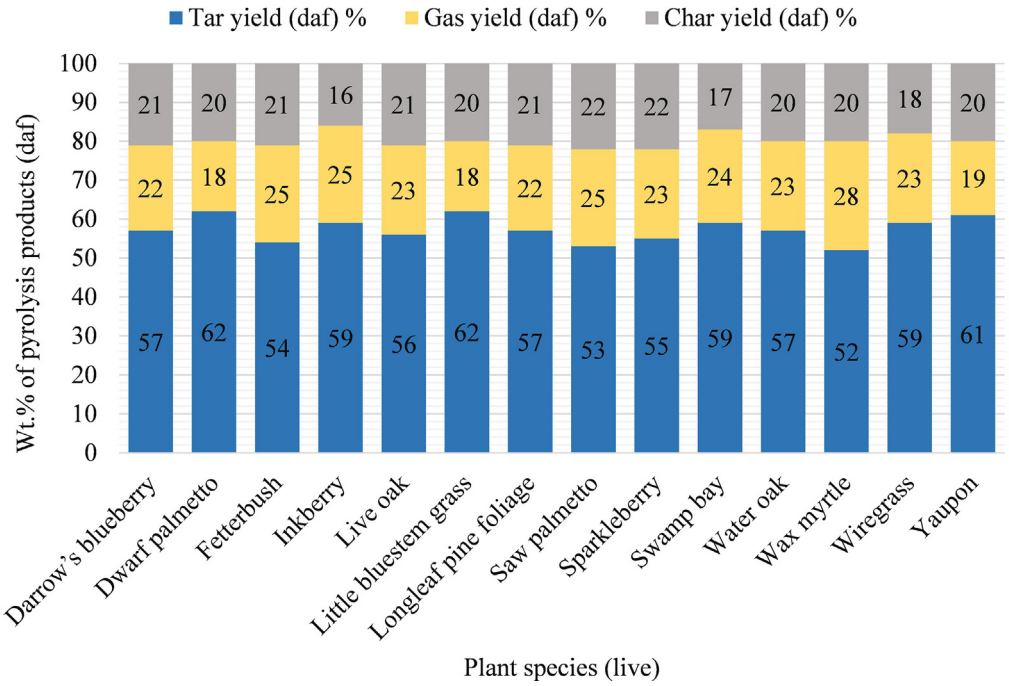

Fig. 4. Product yields of live plant species on a dry, ash-free (daf) basis.

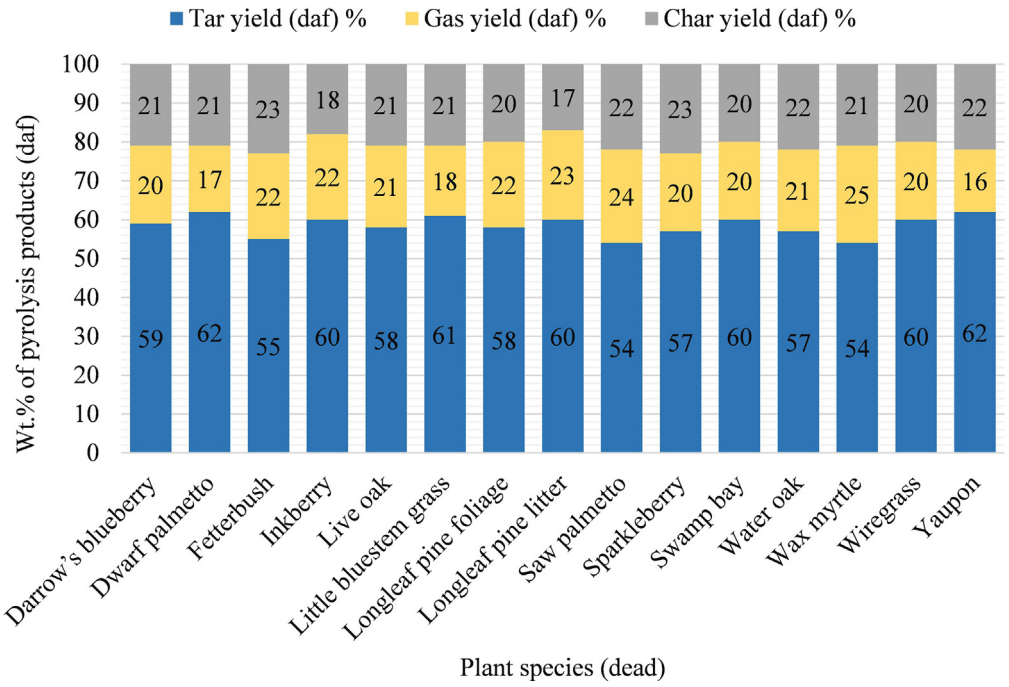

Fig. 5. Product yields of dead plant species on a dry, ash-free (daf) basis.

total heat flux during the experiments. The total heat flux at the position of the plant species was measured to be 100 kW m^{-2}, with less than 5% due to radiation. The total heating rate was estimated to be approximately 100 °C s^{-1} (as reported by Engstrom et al. [31]). This heating rate and heat flux provide a high heating rate pyrolysis condition similar to what has been observed in wildland fires. The FFB was equipped with a cooling water recirculation system to prevent overheating and potential damage, which kept the burner surface cool enough that radiation from the burner to the sample was negligible. The burner surface temperature, as measured by a thermocouple at various locations, was 80 ± 5 °C. The gaps between the burner and glass walls were filled with zirconia felt to prevent oxygen from entering the system.

The gases within the FFB were analyzed continuously with GC-TCD to insure there was no O_2 in the system. The total mass of the samples was weighed before loading samples into the FFB by using a Denver Instrument A-200DS balance. Then the samples were attached to a horizontal rod using a clip. The rod was attached to a Mettler Toledo XS204 scale which recorded the mass at a data rate of 50 Hz using LabVIEW software. The FFB structure was placed on wheels and was equipped with a conveyor belt which enabled the structure to be moveable. After loading the sample, the burner was pulled into position to stop under the sample. The vertical distance between the burner and the sample was 26 cm. In addition, plant surface temperature was recorded by an FLIR A-300 Series infrared camera, and the data analysis

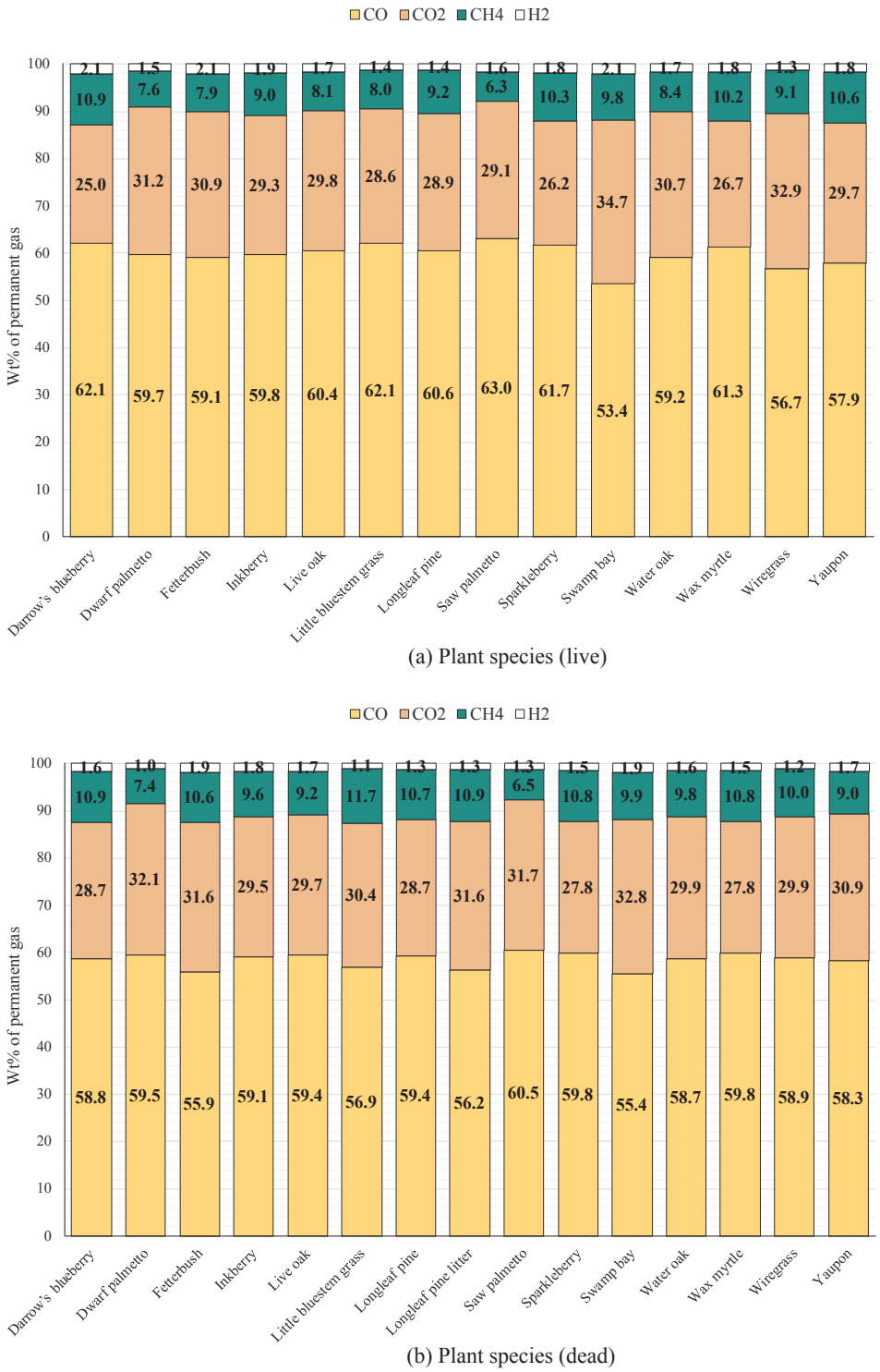

Fig. 6. Light gas species analysis for (a) live plants and (b) dead plants.

was performed using FLIR ResearchIR Max 4 software. Additional details can be found in Safdari [32].

As illustrated in Fig. 2, the sample was placed below a funnel into which the pyrolysis gases were pulled using an oil-less Air Cadet vacuum pump. The distance between the sample and the top of the funnel was 10 cm. The velocity of the gases at the location of the plant sample was 1 m s^{-1}. The estimated residence time of pyrolysis gases between the sample and the top of the funnel was 100 ms. After entering the funnel, the pyrolysis gases flowed through a transfer line that was held at a temperature of 300 °C using heating tape to avoid the condensation of heavy hydrocarbons in the line. Several thermocouples were placed along the heated transfer line to record the temperature. In order to collect condensable pyrolysis products (tars), the pyrolysis gases then flowed through a series of test tubes which were filled with glass wool and placed inside an ice bath. The light gases were then collected in 5 L Tedlar® bags which were placed at the end of the process line. Upon the completion of the experiments, light gases were then analyzed off-line using a ThermoFisher Scientific Trace 1310 gas chromatograph equipped with Chrompack Molsieve5A (25 m × 0.32 mm × 30 μm) and TracePLOT TG-Bond Q (30 m × 0.32 mm × 10 μm) columns and a

Table 4
Average light gas compositions of all plant species.

Gas Species	Live (wt% dry)	Dead (wt% dry)
CO	59.8	58.4
CO_2	29.6	30.2
CH_4	9.0	9.8
H_2	1.7	1.5

thermal conductivity detector (GC-TCD). The oven temperature was programmed to hold the sample at 40 °C for 3 min, then heated to 250 °C at 10 °C min^{-1}, and then held at 250 °C for 4 min. Helium was used as a carrier gas and the size of the sample was 10.0 μL with a split ratio of 25 [33]. Furthermore, the glass wool was removed from the test tubes and placed in a beaker. Tars were extracted from the glass wool and the sides of the test tubes using dichloromethane (DCM) as a solvent. About 2 g of anhydrous $CaSO_4$ powder was added to the DCM/tar solution to absorb any H_2O present. The decanted DCM/tar solution was then analyzed off-line by an HP 5890 gas chromatograph equipped with a Restek Rxi-1ms capillary column (60 m × 0.25 mm × 1 μm) and an HP 5972 mass spectrometer (GC–MS). The oven temperature was programmed to hold the sample at 50 °C for 5 min, then heated to 310 °C at 10 °C min^{-1}, and held at 310 °C for 5 min. Helium was used as a carrier gas, and the size of the sample was 1.0 μL with a split ratio of 10 [34]. After each experimental run, the line, test tubes, and the funnel were cleaned using acetone and dichloromethane as solvents in order to remove contaminants and prepare the setup for the next experiments.

2.5. Statistical analysis

All experiments, including light gas and tar analysis were repeated three times. ANOVA data analysis tool in Microsoft Excel 2017 was used and the results are expressed as arithmetic mean values with a ± 95% confidence interval [35].

3. Results and discussion

3.1. Pyrolysis product yields

Distribution of pyrolysis products (tar, light gas, and char) is influenced by several factors such as: operating temperature, heating rate, reactor type, solid residence time, solid particle size, and etc. [7]. Figs. 4 and 5 illustrate the distribution of pyrolysis products for live and dead plant species in the FFB apparatus, respectively. The results are the average of three experiments and are expressed on a dry ash-free basis. The data reproducibility was excellent, with a standard deviation of less than 5%. The char yields were obtained from the final mass of the solid residue. The tar yields were determined by finding the difference between the initial mass of the test tubes and the final mass. The gas yields were determined by difference.

Tar yields were in the range of 52–62 wt% for live plants, and 54–62 wt% for dead plants. Gas yields were in the range of 18–28 wt% for live plants, and 17–24 wt% for dead plants. Char yields varied between 16 and 22 wt% for live plants, and 17–23 wt% for dead plants. There was not a significant difference in pyrolysis product yields between live and dead samples for a specific plant species; the largest differences in both tar yield (3 wt%) and char yield (4 wt%) were found between live longleaf pine and dead longleaf litter. The swamp bay showed the largest difference in gas yield (4 wt%) between the live and dead samples. Variation in pyrolysis product yields can be caused by changes in the composition of plants as well as the interaction of the plant constituents (cellulose, hemicellulose, and lignin) [36]. However, none of the differences in yields of tar, light gas, or char for live and dead samples for a given species seem more than 5 relative % different in these experiments.

3.2. Light gas analysis

The major post-flame gas analysis from the flat-flame burner using the GC-TCD was 69.7 mol% N_2, 19.9 mol% H_2O, 6.1 mol% CO_2, 3.1 mol % CO, and 1.7 mol% H_2. This background was subtracted in order to find the actual concentration of light gases from the pyrolysis of plant species. The measured composition of light gas species for both live and dead plants are shown in Fig. 6 on a dry (H_2O-free) basis. Weight fraction here means the ratio of the mass of gas to the total mass of gases collected in the gas collection bag. All other species seemed to be below the detection limit of the GC-TCD system. Light gas species data are presented on a wt% basis in order to correlate with the light gas yield, which is also on a mass basis. The results are the average of three tests. The average relative confidence intervals (i.e., the confidence interval divided by the mean) for the live plant analysis were 12%, 7%, 12%, and 18% for H_2, CO, CO_2, and CH_4, respectively. Similar relative confidence intervals were obtained for the dead plant species analysis.

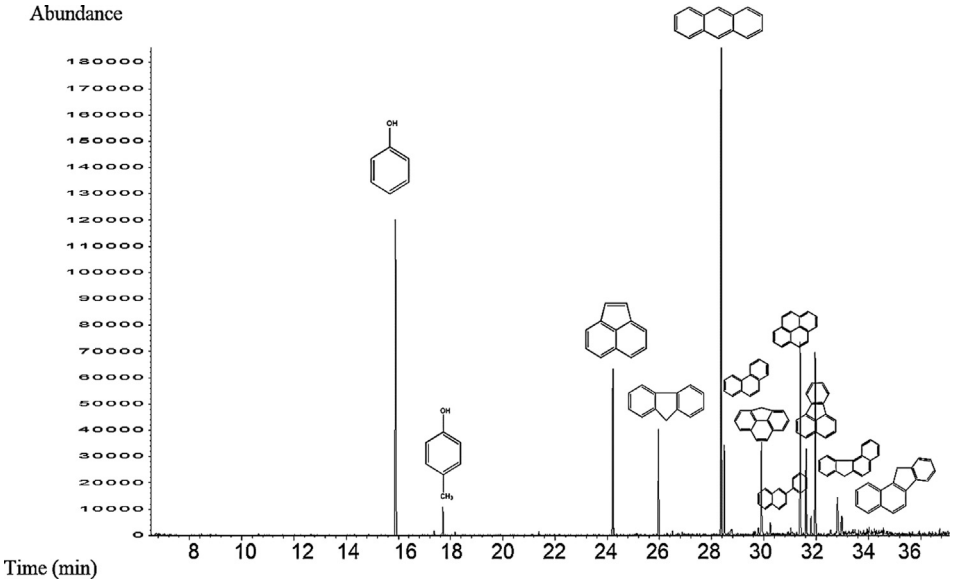

Fig. 7. GC–MS chromatogram of tar from high-heating rate pyrolysis of live inkberry in FFB.

Carbon monoxide is the main component in the light gases on a wt% dry basis, followed by CO_2, CH_4, and H_2. The wt% of CO was between 53–63% for live plants, and 55–60% for dead plants. The little bluestem grass demonstrated the highest statistically significant difference in CO (5.16 wt%) between the live and dead samples (P value < 0.05). Longleaf pine litter, Darrow's blueberry, and fetterbush exhibited the next highest live vs. dead differences in CO of 4.36 wt%, 3.34 wt%, and 3.19 wt%, respectively. The high CO concentration is attributed to a decarbonylation reaction at high heating rates and temperatures [37].

Carbon dioxide was the second most abundant light gas. CO_2 composition varied between 25 and 34 wt% for live plants, and between 27 and 32 wt% for dead plants. The largest statistically significant difference in the weight percent of CO_2 between live and dead samples (P < 0.05) was observed in the Darrow's blueberry (3.71 wt %), followed by the longleaf pine litter (2.72 wt%) and the saw palmetto (2.61 wt%). At high heating rates and temperatures, CO_2 is formed mainly by lignin degradation. Formation of CO_2 is also due to a decarboxylation reaction, especially at lower temperatures [38].

Methane comprised about 6–11 wt% (dry) of light gases in live plants. This range was 6–12 wt% for dead plants. The largest statistically significant difference in CH_4 composition between live and dead samples (P < 0.05) was observed in the little bluestem grass (3.66 wt %), the fetterbush (2.72 wt%), and the longleaf pine litter (1.68 wt%). At high pyrolysis temperatures, CH_4 mainly forms due to the splitting of C-O bonds during lignin degradation as well as removal of methoxy groups from the aromatic rings [39].

H_2 yield varied between 1 and 2 wt% (dry). Among all the plant species, the dwarf palmetto exhibited the highest statistically significant difference (P < 0.05) in H_2 weight percent (0.46 wt%) between the live and dead samples. The next largest differences were found in the Darrow's blueberry (0.41 wt%) and the saw palmetto (0.33 wt%). The formation of H_2 is caused by dehydrogenation during pyrolysis. Hydrogen can form by two mechanisms at high pyrolysis temperatures: first, the decomposition of phenolic groups in lignin; and second, the secondary reactions of heavy gaseous hydrocarbons, which causes cracking and the rearrangement of aromatic bonds [37,39].

In most of the cases, weight fractions of CO and H_2 were slightly higher in pyrolysis of live plants than that of the dead plants. In contrast, weight fractions of CO_2 and CH_4 were slightly higher in pyrolysis of dead plants. It is interesting that the length of aging of the longleaf pine needles did not have a large effect on any of the light gas yields (changes of less than 5 wt% for any major light gas species).

It is interesting that the changes in the light gas species for little bluestem grass, longleaf pine litter, and Darrow's blueberry were the most statistically significant between live and dead samples. Changes in the light gas species for the other plant species were not statistically consistent. From a combustion perspective, the differences in the H_2 wt % among all species, live or dead, seemed minor. The swamp bay sample showed an observable difference in CO and CO_2 from the rest of the plant species. For the most part, it may be reasonable to assume an average composition of light gases (on a dry basis) for live or dead plant species, as shown in Table 4.

3.3. Tar analysis

Tar is defined here as the mixture of pyrolyzed hydrocarbons that condensed in the cold trap. Biomass tars generally consist of a complex mixture of 1- to 5-ring aromatic compounds made up of oxygen-containing hydrocarbons and polycyclic aromatic hydrocarbons [40,41]. Tars can be classified into five subclasses based on their solubility and condensability: (1) heterocyclic aromatic compounds with high solubility (e.g. pyridine); (2) light single-ring aromatic compounds (e.g. toluene); (3) light polycyclic aromatic compounds with 2–3 rings (e.g. naphthalene); (4) heavy polycyclic aromatic compounds with 4–7 rings (e.g. pyrene); (5) very heavy tars which are not detectable by gas chromatography [41,42].

During the experiments in the FFB, the pyrolysis liquids (tars) which were condensed and collected in the ice bath were brownish. The tars then were extracted by dichloromethane as a solvent and analyzed using GC–MS. The majority of the identified tar from high heating rate pyrolysis includes compounds that are composed of 1- to 5-ring aromatics with very few attachments. Fig. 7 illustrates the chromatogram of tar analysis for live inkberry that was pyrolyzed in the FFB apparatus and then analyzed by the GC–MS instrument. This is one example of more than 90 tar analysis experiments that were performed on pyrolysis of live and dead vegetation. Table 5 shows a list of tar compounds which were identified by GC–MS during high-heating rate pyrolysis of live (L) and dead (D) plant species in the FFB apparatus.

Table 5
Identified compounds in tar analysis using GC–MS.

Compound No.	Peak retention time (min)	Compound name	Chemical class	Compound type	Molecular formula	Structure
1	12.636	2-Cyclopenten-1-one	Alkene	Oxygenated	C_5H_6O	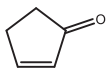
2	12.697	Furfural	Aldehydes	Monocyclic aromatic	$C_5H_4O_2$	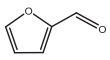
3	12.986	2-Pentanone, 4-hydroxy-4-methyl-	Ketones	Oxygenated	$C_6H_{12}O_2$	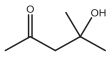
4	13.260	2-Furanmethanol	Alcohols	Monocyclic aromatic	$C_5H_6O_2$	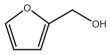
5	14.050	2(3H)-Furanone	Ketones	Monocyclic aromatic	$C_4H_4O_2$	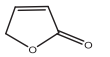
6	14.540	Ethanone, 1-(2-furanyl)-	Ketones	Monocyclic aromatic	$C_6H_6O_2$	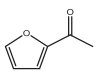
7	14.730	1,2-Cyclopentanedione	Ketones	Oxygenated	$C_5H_6O_2$	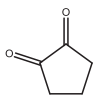
8	15.132	3-Heptyne, 5-methyl-	Alkynes	Aliphatic	C_8H_{14}	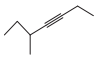

(continued on next page)

Table 5 (*continued*)

Compound No.	Peak retention time (min)	Compound name	Chemical class	Compound type	Molecular formula	Structure
9	15.218	Pyridazine	Pyridines	Heterocyclic aromatic	$C_4H_4N_2$	
10	15.296	2,3-Pentanedione	Ketones	Aliphatic	$C_5H_8O_2$	
11	15.563	4H-Pyran-4-one	Ketones	Heterocyclic aromatic	$C_5H_4O_2$	
12	15.585	2-Furancarboxaldehyde, 5-methyl-	Aldehydes	Monocyclic aromatic	$C_6H_6O_2$	
13	15.876	Phenol	Phenols	Monocyclic aromatic	C_6H_6O	
14	16.183	2-Penten-1-ol, 2-methyl-	Alcohols	Oxygenated	$C_6H_{12}O$	
15	16.868	1,2-Cyclopentanedione, 3-methyl-	Ketones	Oxygenated	$C_6H_8O_2$	
16	17.076	Benzyl Alcohol	Alcohols	Monocyclic aromatic	C_7H_8O	
17	17.712	Phenol, 4-methyl-	Phenols	Monocyclic aromatic	C_7H_8O	
18	17.383	Phenol, 2-methyl-	Phenols	Monocyclic aromatic	C_7H_8O	
19	17.805	1-Octen-3-ol	Alcohols	Oxygenated	$C_8H_{16}O$	
20	18.172	Phenol, 2-methoxy- (guaiacol)	Phenols	Monocyclic aromatic	$C_7H_8O_2$	
21	19.071	Phenol, 3,4-dimethyl-	Phenols	Monocyclic aromatic	$C_8H_{10}O$	
22	19.312	Phenol, 4-ethyl-	Phenols	Monocyclic aromatic	$C_8H_{10}O$	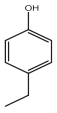
23	19.635	1,2-Benzenediol	Phenols	Monocyclic aromatic	$C_6H_6O_2$	
24	19.948	1,3-Benzenediol, 4-ethyl-	Phenols	Monocyclic aromatic	$C_8H_{10}O_2$	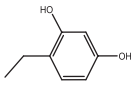
25	20.047	Naphthalene	Benzenoid	Polycyclic aromatic	$C_{10}H_8$	
26	20.058	Benzofuran, 2,3-dihydro-	Furans	Monocyclic aromatic	C_8H_8O	
27	20.611	1,4-Benzenediol	Phenols	Monocyclic aromatic	$C_6H_6O_2$	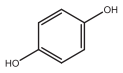
28	20.726	1,2-Benzenediol, 3-methyl-	Phenols	Monocyclic aromatic	$C_7H_8O_2$	
29	20.891	Quinoline	Benzenoid	Heterocyclic aromatic	C_9H_7N	
30	21.004	1,2-Benzenediol, 3-methoxy-	Phenols	Monocyclic aromatic	$C_7H_8O_3$	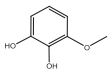
31	21.132	1,2-Benzenediol, 4-methyl-	Phenols	Monocyclic aromatic	$C_7H_8O_2$	
32	21.322	Phenol, 4-ethyl-2-methoxy-	Phenols	Monocyclic aromatic	$C_9H_{12}O_2$	

(*continued on next page*)

Table 5 (*continued*)

Compound No.	Peak retention time (min)	Compound name	Chemical class	Compound type	Molecular formula	Structure
33	21.429	Indole	Benzenoid	Heterocyclic aromatic	C_8H_7N	
34	21.786	Ethanone, 1-(2-hydroxy-5-methylphenyl)-	Ketones	Monocyclic aromatic	$C_9H_{10}O_2$	
35	21.940	2-Methoxy-6-methylphenol	Phenols	Monocyclic aromatic	$C_8H_{10}O_2$	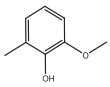
36	22.146	Phenol, 2,6-dimethoxy-	Phenols	Monocyclic aromatic	$C_8H_{10}O_3$	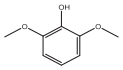
37	22.366	1,2,3-Benzenetriol	Phenols	Monocyclic aromatic	$C_6H_6O_3$	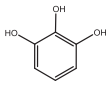
38	22.535	1,2-Benzenediol, 4-ethyl-	Phenols	Monocyclic aromatic	$C_8H_{10}O_2$	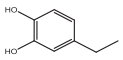
39	23.025	Benzene ethanol, 4-hydroxy-	Phenols	Monocyclic aromatic	$C_8H_{10}O_2$	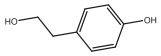
40	23.495	1-Methylnaphthalene	Benzenoid	Polycyclic aromatic	$C_{11}H_{10}$	
41	23.736	1,2,3-Benzenetriol, 5-methyl-	Phenols	Monocyclic aromatic	$C_7H_8O_3$	
42	24.196	Acenaphthylene	Benzenoid	Polycyclic aromatic	$C_{12}H_8$	
43	24.559	2-Methylnaphthalene	Benzenoid	Polycyclic aromatic	$C_{11}H_{10}$	
44	25.941	Fluorene	Benzenoid	Polycyclic aromatic	$C_{13}H_{10}$	
45	26.877	Naphthalene, 2,6-diisopropyl-	Benzenoid	Polycyclic aromatic	$C_{16}H_{20}$	
46	28.352	Anthracene	Benzenoid	Polycyclic aromatic	$C_{14}H_{10}$	
47	28.473	Phenanthrene	Benzenoid	Polycyclic aromatic	$C_{14}H_{10}$	
48	29.898	4H Cyclopenta[def]phenanthrene	Benzenoid	Polycyclic aromatic	$C_{15}H_{10}$	
49	30.237	Naphthalene, 2-phenyl-	Benzenoid	Polycyclic aromatic	$C_{16}H_{12}$	
50	31.378	Fluoranthene	Benzenoid	Polycyclic aromatic	$C_{16}H_{10}$	
51	31.762	Benzo[e]pyrene	Benzenoid	Polycyclic aromatic	$C_{20}H_{12}$	
52	31.992	Pyrene	Benzenoid	Polycyclic aromatic	$C_{16}H_{10}$	
53	32.935	7H-Benzo[c]fluorene	Benzenoid	Polycyclic aromatic	$C_{17}H_{12}$	
54	32.979	11H-Benzo[a]fluorene	Benzenoid	Polycyclic aromatic	$C_{17}H_{12}$	
55	34.732	Benzo[c]phenanthrene	Benzenoid	Polycyclic aromatic	$C_{18}H_{12}$	
56	34.889	Benzo(a)fluoranthene	Benzenoid	Polycyclic aromatic	$C_{20}H_{12}$	
57	34.941	Cyclopenta[cd]pyrene	Benzenoid	Polycyclic aromatic	$C_{18}H_{10}$	
58	35.430	Naphthacene	Benzenoid	Polycyclic aromatic	$C_{18}H_{12}$	
59	35.517	Benz(a)anthracene	Benzenoid	Polycyclic aromatic	$C_{18}H_{12}$	
60	35.988	Chrysene	Benzenoid	Polycyclic aromatic	$C_{18}H_{12}$	

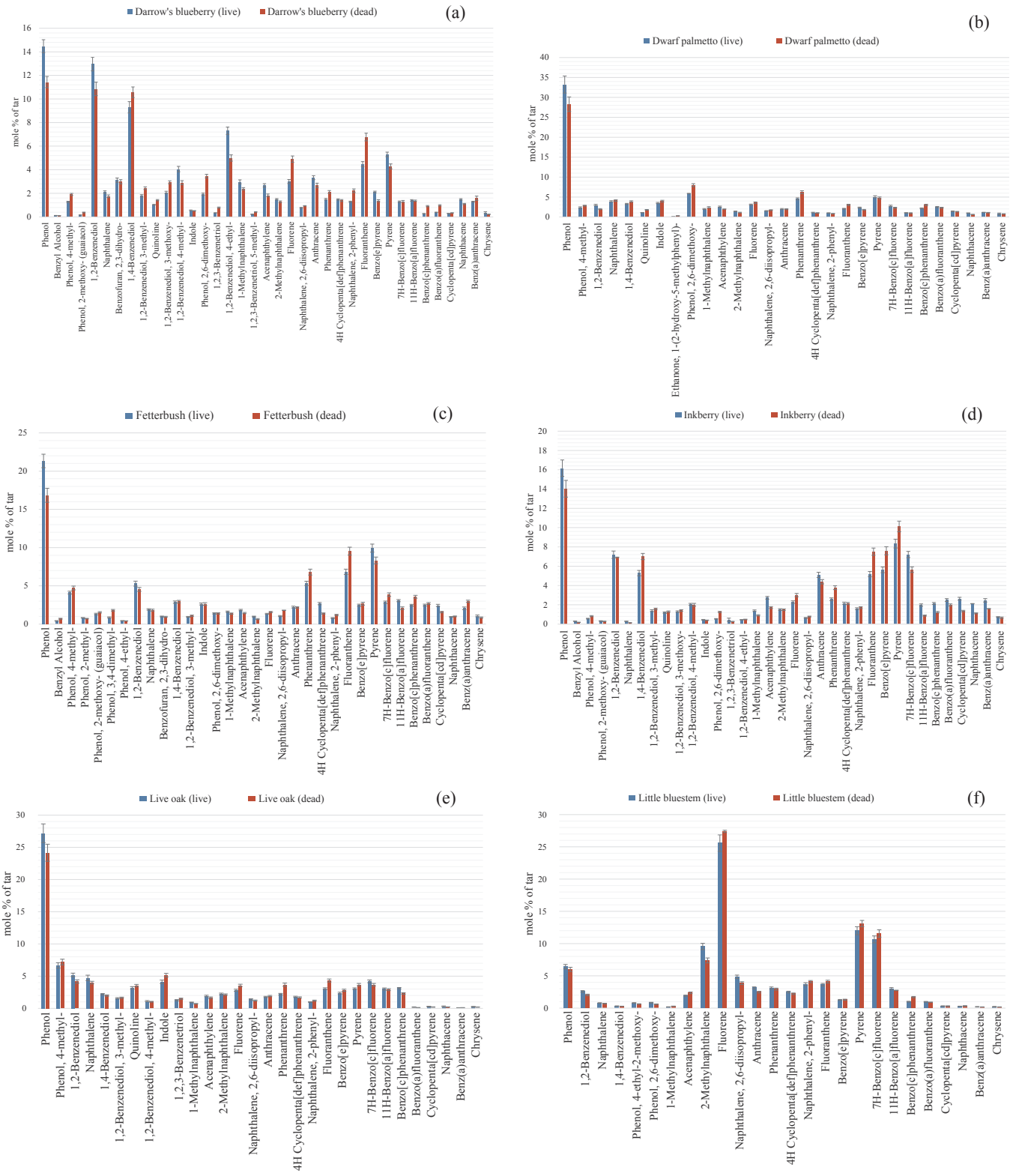

Fig. 8. Analysis of tar compounds for live versus dead plant species.

The results of tar analysis from fast pyrolysis of live versus dead plant species are shown in Fig. 8. Identified tar compounds and the average of their relative peak area, which represent mole fraction in tar samples, are shown. Mole fractions are shown because there may be some compounds that were too heavy to detect in the GC–MS system. The error bars represent the ± 95% confidence intervals for three tests. The results of tar analysis for live and dead longleaf pine foliage, along with longleaf pine litter (pine straw), are shown in Fig. 8g. For brevity, tar species with 0.0 mol% are not shown in this figure.

During high heating rate pyrolysis of both live and dead plants, 1- to 5-ring compounds were observed with very few attachments on the rings. Phenol, naphthalene, fluorene, anthracene, phenanthrene, fluoranthene, and pyrene were the major identified tar compounds. Differences in tar composition were observed for each plant species. For

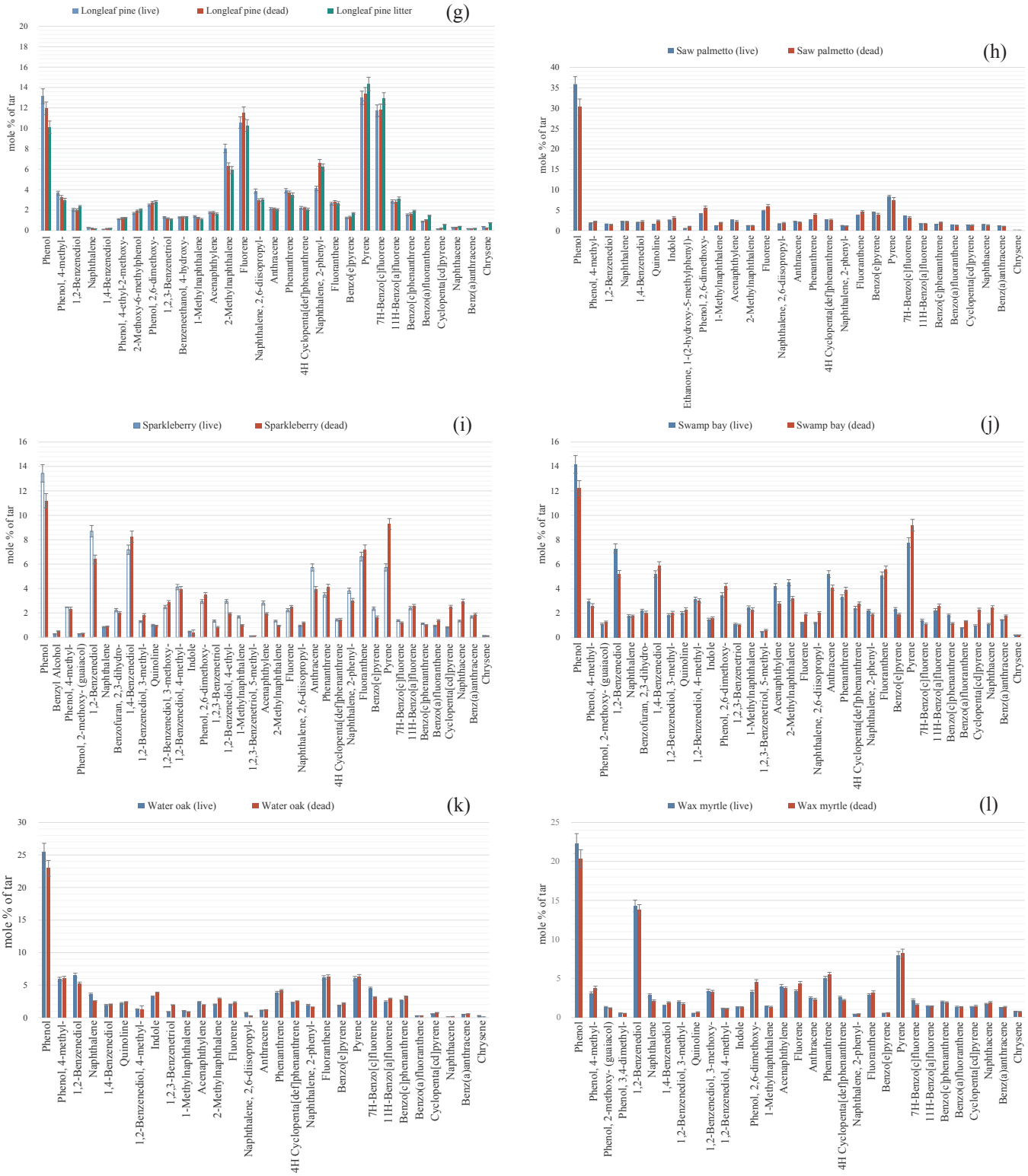

Fig. 8. (*continued*)

example, in tar analysis, phenol ranged from 6 mol% in dead little bluestem grass to 36 mol% in live saw palmetto. Two plants from the same family, saw palmetto and dwarf palmetto, showed the highest phenol formation at 36% and 33 mol%, respectively. The grasses (little bluestem and wiregrass) and needle-like species (i.e., longleaf pine) exhibited the lowest concentrations of phenol with 6%, 10%, and 13 mol%, respectively. In grasses, higher concentrations of fluorene (12–27 mol%) and pyrene (7–14%) were observed compared to the rest of the plant species. Phenolic compounds were generally the main constituents of tar. Phenolic compounds, such as 4-methyl phenol, 2-methoxy phenol (guaiacol), and 3,4-dimethyl phenol, mainly form by the depolymerization of lignin building blocks [39,43].

3.4. Tar formation mechanisms

Lignin is highly reactive due to the presence of phenolic hydroxyl

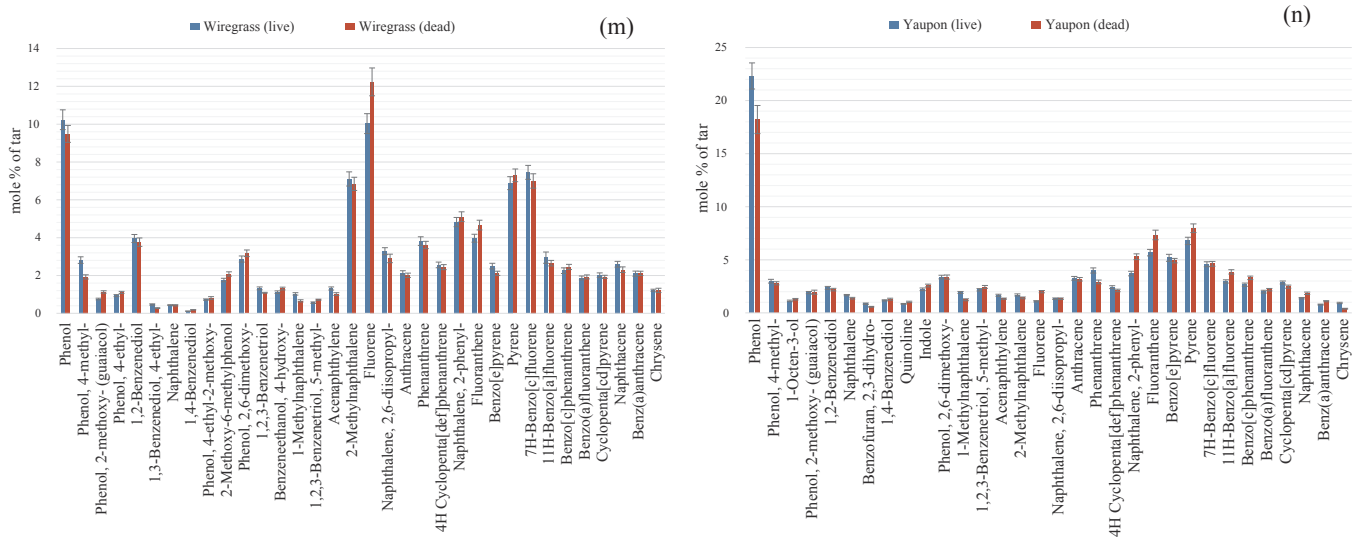

Fig. 8. (*continued*)

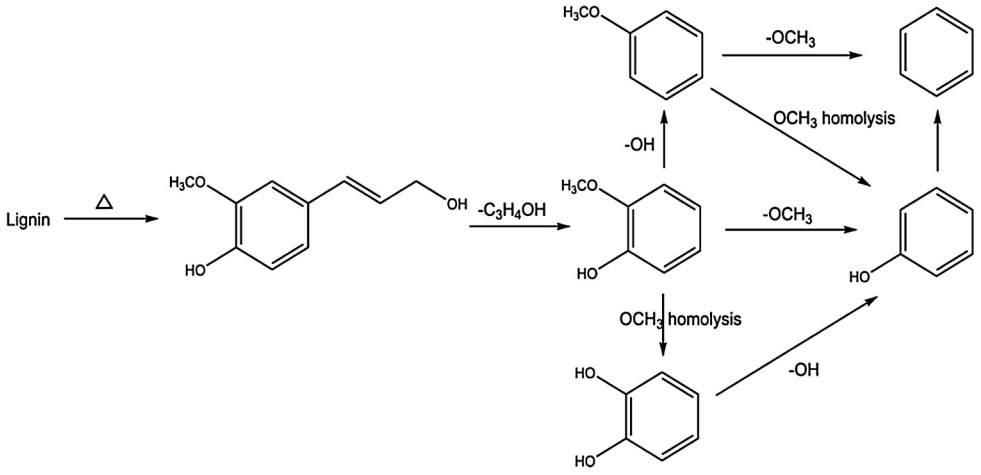

Fig. 9. Mechanisms of PAH precursor formation from lignin decomposition [45].

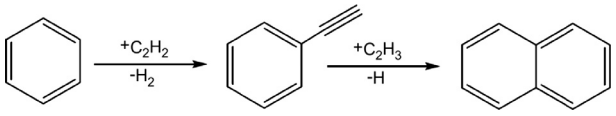

Fig. 10. Mechanism of formation of naphthalene from benzene [8].

and methoxyl groups in its chemical structure. Lignin decomposition leads to the formation of single-ring, low molecular weight aromatics [44]. Fig. 9 indicates a proposed mechanism of lignin decomposition and formation of polycyclic aromatic hydrocarbon (PAH) precursors [22]. This mechanism explains the presence of the many phenolic compounds observed in Fig. 8.

The presence of multi-ring compounds in Fig. 8 is related to the formation of naphthalene from benzene (with phenylacetylene as a possible intermediate via hydrogen abstraction acetylene addition) as shown in Fig. 10 [8].

The heavier polycyclic aromatic hydrocarbons (PAHs) of 3+ rings in Fig. 8 can form from naphthalene via various mechanisms. For example, acenaphthylene can evolve by the addition of acetylene to naphthalene [46]. The presence of furans (and their derivatives) in tar is mainly believed to be from hemicellulose, and the evolution of carbonyl and carboxylic groups are from the pyrolysis of cellulose [47,48]. These mechanisms may explain the presence of the tar species in Fig. 8 with oxygen in the ring or C=O groups.

3.5. Distribution of functional groups in tar

Fig. 11 shows the distribution of functional groups in tar for four plant species as an example of more than 90 tar analysis experiments that were performed on pyrolysis of live and dead vegetation. These plant species were chosen to be representative of palmetto-type, broadleaf, grass, and needle-like species.

There is only a small difference between the distribution of functional groups in tar for live and dead plant species. For example, phenols comprised 48% and 45% of the tar from live and dead dwarf palmetto, respectively. Three-ring aromatics comprise 13% of the tar from live dwarf palmetto vs. about 15 mol% from dead dwarf palmetto. This trend of small differences in the yields of functional groups for live vs. dead samples was observed in all plant species. For the majority of the live plants, slightly more phenol, anthracene, pyrene, and 1,2-benzenediol formed during pyrolysis. On the other hand, slightly more 1,4-benzenediol, fluorene, phenanthrene, and fluoranthene evolved during the pyrolysis of dead plants.

In contrast, when comparing tar compounds from different plant species a significant difference in the distribution of functional groups was observed. For live inkberry (a broad-leaf plant), the tar consisted of more than 35 mol% phenolic compounds and 60 mol% polycyclic aromatic hydrocarbons, which included about 4% 2-ring, 14% 3-ring, 32% 4-ring, and 10% 5-ring aromatics. For needle-like plants such as live

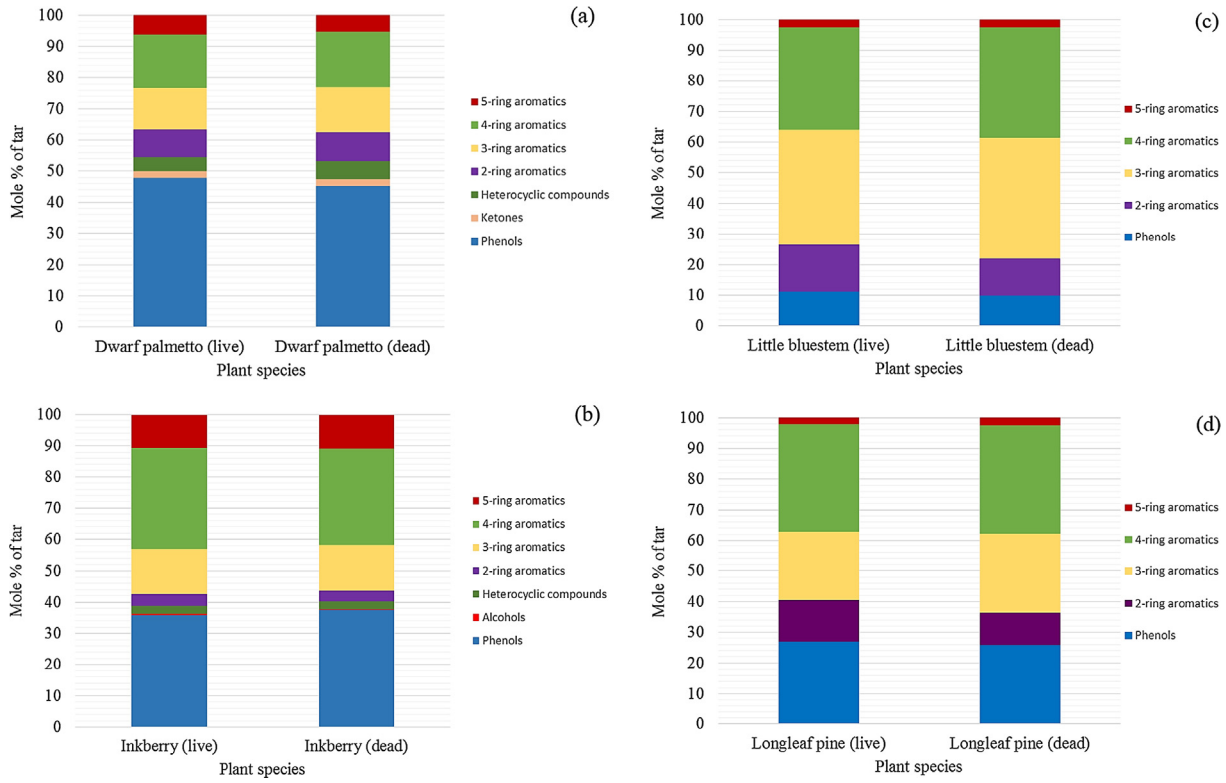

Fig. 11. Distribution of functional groups in tar for live and dead plants.

longleaf pine, the functional group distribution was noticeably different from live broad-leaf plants. In live longleaf pine, about 26% and 73 mol % of the tar were phenols and polycyclic aromatics, respectively. In contrast, phenols and polycyclic aromatics were 11% and 89 mol% in the little bluestem grass, which seems to be evidence of different distributions of functional groups in tar from pyrolysis of plant species.

4. Conclusion

Fast pyrolysis of 14 live and dead plant species which are native to the Southern United States were studied using a fuel-rich flat-flame burner (FFB) apparatus. Distribution of pyrolysis products was investigated using GC–MS for analysis of the tars, and GC-TCD for analysis of the light gases.

The main conclusions from this research are listed as follows:

1- Tar yields for live plants ranged from 52 to 62 wt% (dry basis), and corresponding light gas yields ranged from 18 to 28 wt%.
2- There was only a slight difference in pyrolysis product yields between live and dead samples for a specific plant species.
3- Carbon monoxide was the main component in the light gases on a wt % dry basis, followed by CO_2, CH_4, and H_2. For most plant species, weight fractions of CO and H_2 were slightly higher in pyrolysis of live plants than that of the dead plants. In contrast, weight fractions of CO_2 and CH_4 were slightly greater in pyrolysis of dead plants.
4- Most plant species from the same type of plant (broadleaf, grass, or needle-like) showed only small differences in yields of the light gases (CO, CO_2, CH_4, and H_2).
5- Tar compounds from high heating rate pyrolysis of both live and dead plants consisted of 1- to 5-ring compounds with very few attachments on the rings. Major tar species observed included phenol, naphthalene, fluorene, anthracene, phenanthrene, fluoranthene, and pyrene.
6- For a given plant species, there was only a small difference between the distribution of functional groups in tar for live and dead plants. For the majority of the live plants, slightly more phenol, anthracene, pyrene, and 1,2-benzenediol formed during pyrolysis. On the other hand, slightly more 1,4-benzenediol, fluorene, phenanthrene, and fluoranthene evolved during the pyrolysis of dead plants.
7- Tar compounds from different plant species exhibited a significant difference in the distribution of functional groups. The greatest concentrations of phenolic compounds were observed in the broadleaf species, with especially high concentrations in the palmetto species. However, for needle-like plants such as longleaf pine, fewer phenolic compounds were observed in the tar but more 3-ring compounds were observed. The tars from grass species had very little phenolic compounds, but increased levels of 3- and 4-rings compounds.

These data can be used to find the heat release and investigate reactions that occur during the fast pyrolysis and subsequent combustion of live and dead vegetation. Finding mechanisms of formation of pyrolysis products will likely help to prepare more accurate models to predict the best conditions to properly perform prescribed burning, predict fire propagation, and limit fire runaway.

Acknowledgements

This research was funded by DOD/EPA/DOE Strategic Environmental Research and Development Program, Project RC-2640, funded through contract 16-JV-11272167-024, administered by the USDA Forest Service PSW Research Station. Fred Matt of the USDA Forest Service Forest Products Lab helped provide the proximate and ultimate analyses of the plant species.

References

[1] McAllister S, Grenfell I, Hadlow A, Jolly WM, Finney M, Cohen J. Piloted ignition of live forest fuels. Fire Saf J 2012;51:133–42.
[2] Tansey K, Gregoire JM, Stroppiana D, Sousa A, Silva J, Pereira JMC, et al. Global burned area estimates from SPOT VEGETATION data. J Geophys Res-Atmos 2000;2004:109.
[3] Ferguson SC, Dahale A, Shotorban B, Mahalingam S, Weise DR. The role of moisture on combustion of pyrolysis gases in wildland fires. Combust Sci Technol 2013;185:435–53.
[4] Hartman G. Forest land management guide: use of prescribed fire. Missouri Department of Conservation; 2005.
[5] Melvin MA. National prescribed fire use survey report. Coalition of prescribed fire councils, inc, 2015.
[6] Biagini E, Tognotti L. A generalized procedure for the devolatilization of biomass fuels based on the chemical components. Energy Fuel 2014;28:614–23.
[7] Aysu T, Kucuk MM. Biomass pyrolysis in a fixed-bed reactor: effects of pyrolysis parameters on product yields and characterization of products. Energy 2014;64:1002–25.
[8] Liu WJ, Li WW, Jiang H, Yu HQ. Fates of chemical elements in biomass during its pyrolysis. Chem Rev 2017;117:6367–98.
[9] Wurzenberger JC, Wallner S, Raupenstrauch H, Khinast JG. Thermal conversion of biomass: comprehensive reactor and particle modeling. AICHE J 2002;48:2398–411.
[10] DiBlasi C. Numerical simulation of cellulose pyrolysis. Biomass Bioenergy 1994;7:87–98.
[11] Bridgwater AV. Review of fast pyrolysis of biomass and product upgrading. Biomass Bioenergy 2012;38:68–94.
[12] Bradbury AW, Sakai Y, Shafizadeh F. A kinetic model for pyrolysis of cellulose. J Appl Polym Sci 1979;23:3271–80.
[13] Diebold JP. A unified, global model for the pyrolysis of cellulose. Biomass Bioenergy 1994;7:75–85.
[14] Rao TR, Sharma A. Pyrolysis rates of biomass materials. Energy 1998;23:973–8.
[15] Dimitrakopoulos AP, Mitsopoulos ID, Gatoulas K. Assessing ignition probability and moisture of extinction in a mediterranean grass fuel. Int J Wildland Fire 2010;19:29–34.
[16] Viney NR. A review of fine fuel moisture modelling. Int J Wildland Fire 1991;1:215–35.
[17] Fletcher TH, Pickett BM, Smith SG, Spittle GS, Woodhouse MM, Haake E, et al. Effects of moisture on ignition behavior of moist California chaparral and Utah leaves. Combust Sci Technol 2007;179:1183–203.
[18] Jolly WM, Johnson DM. Pyro-ecophysiology: shifting the paradigm of live wildland fuel research. Fire 2018;1:8.
[19] Jolly WM, Butler B. Linking photosynthesis and combustion characteristics in live fuels: The role of soluble carbohydrates in fuel preheating, Final Report for JFSP Project ID: 10-1-08-6, Joint Fire Science Program, 2015.
[20] Jolly WM, Hadlow AM, Huguet K. De-coupling seasonal changes in water content and dry matter to predict live conifer foliar moisture content. Int J Wildland Fire 2014;23:480–9.
[21] Yang HP, Yan R, Chen HP, Lee DH, Zheng CG. Characteristics of hemicellulose, cellulose and lignin pyrolysis. Fuel 2007;86:1781–8.
[22] Xiao RR, Yang W. Influence of temperature on organic structure of biomass pyrolysis products. Renewable Energy 2013;50:136–41.
[23] Fourty T, Baret F, Jacquemoud S, Schmuck G, Verdebout J. Leaf optical properties with explicit description of its biochemical composition: direct and inverse problems. Remote Sens Environ 1996;56:104–17.
[24] Sait HH, Hussain A, Salema AA, Ani FN. Pyrolysis and combustion kinetics of date palm biomass using thermogravimetric analysis. Bioresour Technol 2012;118:382–9.
[25] Burling IR, Yokelson RJ, Griffith DWT, Johnson TJ, Veres P, Roberts JM, et al. Laboratory measurements of trace gas emissions from biomass burning of fuel types from the southeastern and southwestern United States. Atmos Chem Phys 2010;10:11115–30.
[26] Barnett JP, McGilvary JM. Practical guidelines for producing longleaf pine seedlings in containers. U.S. Department of Agriculture, Forest Service, Southern Research Station; 1997.
[27] Gallacher J. The influence of season, heating mode and slope angle on wildland fire behavior, Chemical Engineering, Brigham Young University, PhD Dissertation, 2016.
[28] Shen C, Fletcher TH. Fuel element combustion properties for live wildland Utah shrubs. Combust Sci Technol 2015;187:428–44.
[29] Prince D, Shen C, Fletcher T. Semi-empirical model for fire spread in shrubs with spatially-defined fuel elements and flames. Fire Technol 2017;53:1439–69.
[30] Prince DR, Fletcher TH. Differences in burning behavior of live and dead leaves, part 1: measurements. Combust Sci Technol 2014;186:1844–57.
[31] Engstrom JD, Butler JK, Smith SG, Baxter LL, Fletcher TH, Weise DR. Ignition behavior of live California chaparral leaves. Combust Sci Technol 2004;176:1577.
[32] Safdari MS. Characterization of pyrolysis products from fast pyrolysis of live and dead vegetation [PhD Dissertation]. Chemical Engineering Department, Brigham Young University, in progress, 2018.
[33] Safdari MS, Kariminia HR, Nejad ZG, Fletcher TH. Study potential of indigenous *Pseudomonas aeruginosa* and *Bacillus subtilis* in bioremediation of diesel-contaminated water. Water Air Soil Pollut 2017:228.
[34] Fazlollahi F, Saeidi S, Safdari MS, Sarkari M, Klemes JJ, Baxter LL. Effect of operating conditions on cryogenic carbon dioxide removal. Energy Technol-Ger 2017;5:1588–98.
[35] Safdari MS, Kariminia HR, Rahmati M, Fazlollahi F, Polasko A, Mahendra S, et al. Development of bioreactors for comparative study of natural attenuation, biostimulation, and bioaugmentation of petroleum-hydrocarbon contaminated soil. J Hazard Mater 2018;342:270–8.
[36] Zhou H, Wu CF, Meng AH, Zhang YG, Williams PT. Effect of interactions of biomass constituents on polycyclic aromatic hydrocarbons (PAH) formation during fast pyrolysis. J Anal Appl Pyrol 2014;110:264–9.
[37] Gao NB, Liu BL, Li AM, Li JJ. Continuous pyrolysis of pine sawdust at different pyrolysis temperatures and solid residence times. J Anal Appl Pyrol 2015;114:155–62.
[38] Patwardhan PR, Brown RC, Shanks BH. Understanding the fast pyrolysis of lignin. ChemSusChem 2011;4:1629–36.
[39] Xu J, Tahmasebi A, Yu JL. An experimental study on the formation of methoxyaromatics during pyrolysis of eucalyptus pulverulenta: yields and mechanisms. Bioresour Technol 2016;218:743–50.
[40] Phuphuakrat T, Namioka T, Yoshikawa K. Tar removal from biomass pyrolysis gas in two-step function of decomposition and adsorption. Appl Energy 2010;87:2203–11.
[41] Li CS, Suzuki K. Tar property, analysis, reforming mechanism and model for biomass gasification-an overview. Renewable Sustainable Energy Rev 2009;13:594–604.
[42] Shen YF, Wang JF, Ge XL, Chen MD. By-products recycling for syngas cleanup in biomass pyrolysis – an overview. Renewable Sustainable Energy Rev 2016;59:1246–68.
[43] Wang S, Wang Q, Jiang XM, Han XX, Ji HS. Compositional analysis of bio-oil derived from pyrolysis of seaweed. Energy Convers Manage 2013;68:273–80.
[44] Farag S, Fu DB, Jessop PG, Chaouki J. Detailed compositional analysis and structural investigation of a bio-oil from microwave pyrolysis of kraft lignin. J Anal Appl Pyrolysis 2014;109:249–57.
[45] Zhou H, Wu CF, Onwudili JA, Meng AH, Zhang YU, Williams PT. Polycyclic aromatic hydrocarbons (pah) formation from the pyrolysis of different municipal solid waste fractions. Waste Manage 2015;36:136–46.
[46] Palma CF. Model for biomass gasification including tar formation and evolution. Energy Fuel 2013;27:2693–702.
[47] Ku CS, Mun SP. Characterization of pyrolysis tar derived from lignocellulosic biomass. J Ind Eng Chem 2006;12:853–61.
[48] Maggi R, Delmon B. Comparison between slow and flash pyrolysis oils from biomass. Fuel 1994;73:671–7.